15th Australasian Fluid Mechanics Conference
The University of Sydney, Sydney, Australia
13-17 December 2004

Impact of Outlet Boundary Conditions on the Flow Properties within a Cyclone

St. Schmidt, H. M. Blackburn and M. Rudman

CSIRO Manufacturing & Infrastructure Technology
PO Box 56, Highett, Victoria, 3190 AUSTRALIA

Abstract

In this study the influence of the exit tube geometry on the overall flow properties of cyclones is investigated using detached eddy simulation. The results for different exit pipe shapes and lengths reveal that under certain conditions the outlet has an upstream effect on the flow behaviour within the cyclone. This can in turn result in poor build-up of swirl in the crucial region of the cyclone and substantially reduce the efficiency of the cyclone as a particle-separation device.

Introduction

Cyclones are widely used in the industrial cleaning process, where particles are removed from particle-laden carrier flows without the need for using particle filters. The performance of these maintenance-free devices depends to a large extent on the swirl velocity within the cyclone as this quantity directly determines the centrifugal force imposed on the particles and at the same time limits the ability to separate particles from the flow. In cyclone design it is therefore vital to accurately calculate the flow in order to be able to predict the overall performance of the cyclone. The work here deals only with single-phase flow of carrier fluid, as this must be correctly predicted before the solids phase can be considered.

Owing to the technological relevance of cyclones, flow simulations have been carried out in the last decades, as appropriate computational techniques have been developed [1, 2]. Since the Reynolds numbers for cyclone flows are usually in the order of $Re = 10^6$ and the flow itself is inherently very complex due to strong streamline curvature and anisotropic turbulent structures, these flows require sophisticated turbulence modelling in order to obtain reliable and trustworthy results. Of the available models to be applied to the Reynolds-averaged Navier–Stokes (RANS) equations, full Reynolds-stress transport models (RSTM) are best able to cope with turbulence anisotropy and satisfactorily predict these flows [1].

Wall-resolving large eddy simulation (LES), which directly resolves the main turbulent flow structures down to the wall, while potentially the most accurate approach, remains extremely expensive in terms of computational effort and is therefore not useful in product design. However, combinations of RANS and LES, such as detached eddy simulation (DES, [7]) provide attractive alternatives, since this numerical method combines the advantages of LES and RANS. Like LES, DES is capable of resolving unsteady flow features but utilises wall models similar to RANS in order to reduce the spatial resolution in the crucial near-wall region.

Previous results based on LES and DES revealed differences in the flow predictions depending on the inflow conditions, and exhibited deficiency in predicting the swirl level in the cyclonic part of the cyclone [3]. Perhaps more importantly, the results in the present study show that in order to successfully predict flow within the cyclone, care must be paid to the treatment given to the exit tube, downstream of the vortex finder, and external to the cyclone body. It will be demonstrated that the swirl velocity within the cyclone can be influenced dramatically by changing the length and shape of the vortex finder. Highly swirling flows can promote propagation of flow information upstream, against the mean flow direction, by pressure waves, similar to pressure waves in compressible flows [10].

Our results further suggest that the performance of the cyclone in an industrial environment will be greatly influenced by the actual inflow and outflow conditions. Hence, cyclone design should not be restricted to the cyclone itself, but also encompass the surrounding ductwork.

Detached Eddy Simulation

This numerical technique based on the solution of the three-dimensional unsteady Navier–Stokes equations was first introduced by Spalart et al. [7] for the simulation of flows past airfoils at high angles of attack, which feature massive flow separation and the shedding of large vortical structures into the wake.

In terms of numerical modelling, this approach combines methods solving the Reynolds-averaged Navier–Stokes (RANS) equations with large-eddy simulation (LES). Owing to the fact that (like LES) DES resolves the turbulence spectrum up to a certain cut-off wavenumber, it is capable of capturing helical vortices which form around the centreline of a cyclone, a feature common to many swirling flows. At the same time, by avoiding the necessity for fine (eddy-resolving) mesh structure near the walls, DES is substantially cheaper than LES.

From a turbulence modelling point of view, DES is obtained by a slight modification of the destruction term in the Spalart–Allmaras one-equation RANS model [6], resulting in a limitation of the length scale by the grid spacing. This hybrid approach employs the unmodified RANS model in wall areas while turning itself into a one-equation subgrid-scale model in regions located off the wall. The model has been implemented and validated for internal and external high Reynolds number flows [4, 5].

Numerical Method

The Navier–Stokes equations are discretised using a cell-centered finite-volume method based on block-structured grids [11]. All diffusive fluxes are approximated with a central-differencing scheme (CDS). For the convective fluxes, the use of blending functions ensures that in the RANS region a third-order upwind-biased QUICK scheme is used, while in the LES region, CDS is recovered [8]. The time integration is of second order, using a fully implicit three-level scheme, ensuring CFL stability even in coarse regions of the mesh where the CDS would produce unphysical solutions owing to high Peclet numbers. The flow solver is parallelised using a blockwise domain decomposition technique employing message passing library MPI for inter-block communication. Computations were carried out using 28–34 nodes on the APAC Alpha cluster with the same set of boundary conditions, timestep and total integra-

tion time for each configuration, allowing valid comparisons to be made.

Flow Configuration

The cyclone (figure 1a) features an outer diameter $D = 2R$ and a half-angle of $\alpha = 20^\circ$ in the conical region and an underflow-exit pipe at the bottom end for the collection of particles. In this study this outflow is closed for all simulations as only the carrier flow is investigated. Hence only the outflow through the vortex finder with a diameter d at the top of the cyclone is used and convective outflow boundary conditions are imposed on this outlet plane.

All velocities presented here are normalised by the bulk velocity in the inlet duct. The kinematic viscosity of the fluid was set so that the Reynolds number based on this velocity and the cyclone body diameter D was $Re = 1 \times 10^6$, matching the corresponding experiments [9]. Dimensions are normalised by R, and the reference axial location, z_0, is placed in line with the bottom of the cylindrical cyclone outer body. The vortex finder terminates at $z^*/R = (z - z_0)/R \approx 0.5$.

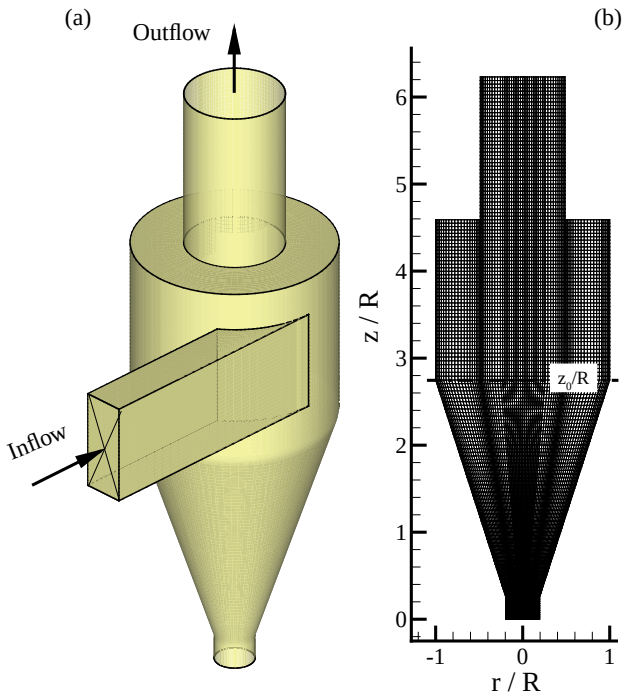

Figure 1: Cyclone geometry and block-structured grid.

Exit Tube Geometries

The results of previous cyclone LES [3] using a spectral-element method on a domain comparable to the one shown in figure 2a, showed a strong under prediction of the swirl velocity component in the cyclone. DES results confirmed that the choice of a short exit tube length (cf. figure 2a) has an adverse effect on the swirl velocity within main part of the cyclone and contributed to the lack of agreement with the experiments [9].

The main goal of this paper is therefore to examine the effects of different outflow geometries on the swirl velocity in the cyclone. The work concentrated on both the extension of the axisymmetric exit tube as well as different outlet geometries, namely a short, medium and long straight exit (figures 2a-c), an outlet with centre-body blocking the core of the flow at the exit (figure 2d), a radial outlet ring surrounding the exit area (figure 2e) as well as a short/long straight pipe with an additional bend and extension tube (figures 2f/g). The original experimental setup included an elongated rectangular inlet duct and a outlet geometry similar to the one depicted in figure 2g.

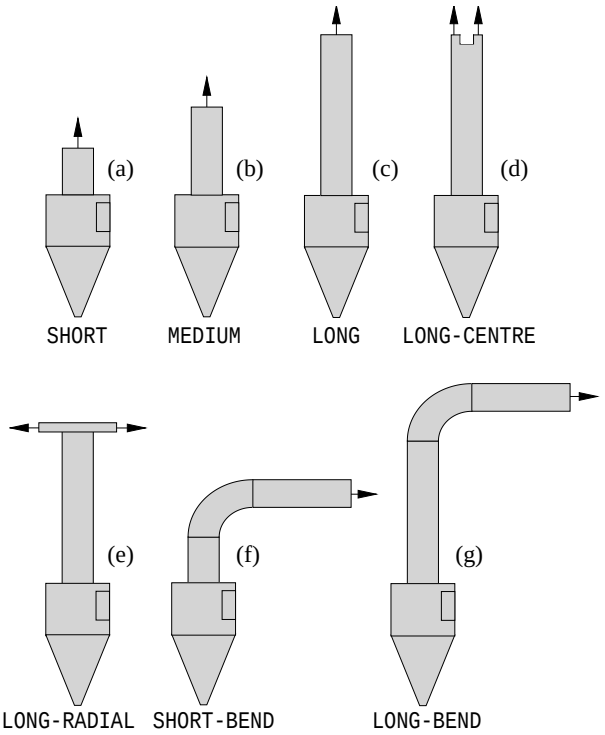

Figure 2: Cyclone outlet geometries: short (a), medium (b) and long (c) straight outlet; long with blocked centre part (d); long with radial outlet (e); short with bend (f) and long outlet with bend similar to the experimental setup (g); arrows indicate outflow direction.

Results

The figures 3a-c show the distribution of the time-averaged swirl velocities at three locations within the cyclone for all geometries including the previously mentioned simulation based on the SHORT geometry (cf. fig. 2a). Obviously the simulations based on geometries with a longer exit are in much closer agreement with the measurements, except the geometry with the long vortex finder and the blocked centre (cf. figure 2d), which gives swirl velocity profiles comparable to those for the SHORT geometry. In part, this setup was chosen because in the previous spectral element LES an axisymmetric centre body was placed in the outlet area in order to prevent any flow re-entering the domain and de-stabilising the numerical scheme. The DES of this configuration suggests that this body slows down the swirl velocity in the cyclone and contributes to the poor quality of the results. Comparing the results of the other geometries, it becomes clear that beyond a certain exit tube length, the shape of the geometry does not have a strong impact on the swirl in the cyclone. Even the inclusion of the bend does not affect the solution significantly.

The mean axial velocities are shown in figures 4a-c. Below the entry plane of the vortex finder (figure 4a) the results are mainly influenced by the length of the exit tube as the solutions tend to approach the results with bend included in the outlet geometry. The shorter the outlet, the more the velocity peak drops and evens out the steep velocity gradients. In the conical part of the cyclone (figure 4b, c) the differences become

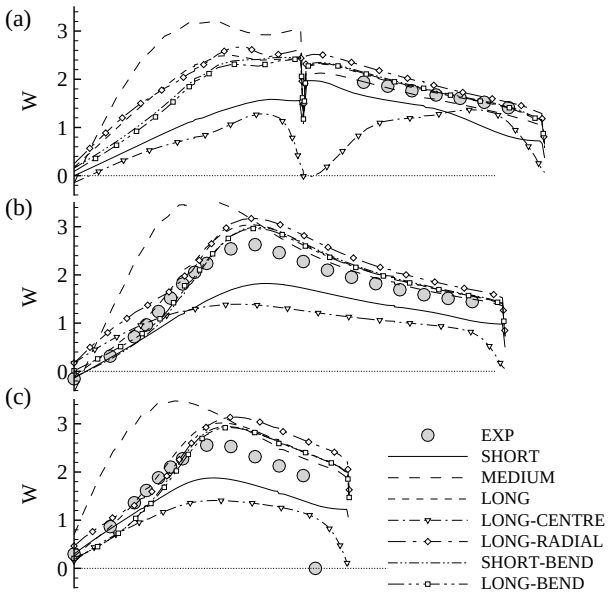

Figure 3: Time-averaged tangential velocity profiles at: (a) $z^*/R = 1.0$, (b) $z^*/R = -0.25$ and (c) $z^*/R = -1.25$.

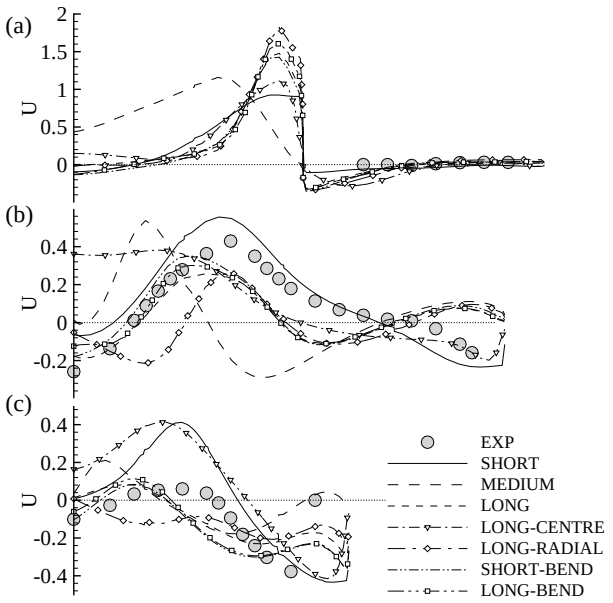

Figure 4: Time-averaged axial velocity profiles at: (a) $z^*/R = 1.0$, (b) $z^*/R = -0.25$ and (c) $z^*/R = -1.25$.

larger and two areas can be identified: a near-axis region, which gives good overall agreement of all solutions, and an internal part, located between the axis and the surrounding walls. In the latter region, the axial velocities of all solutions miss the experiments and tend to flow counter to the experimental results. The computations exhibit three radial locations where the velocity changes direction, whereas the experiments do not suggest such behaviour. As only the solutions where swirl velocities are under-predicted exhibit this behaviour, the results indicate that depending on the swirl more than one flow pattern may exist in the cyclone body.

At the lower end (figure 4c), these differences become more obvious and the geometries with longer exit tubes tend to agree more with the experimental data than the low-swirl solutions.

Influence of Exit Tube Geometry

The differences in the results of the shorter cyclone geometries (`SHORT/MEDIUM`) compared to the other cases can be traced to figure 5, where tangential velocity is represented by grey tones ranging from $W = 0$ (black) to $W = W_{\max}$ (white). The location of the vortex core can be clearly identified as the dark region meandering around the centre line of the cyclone. It can be seen that especially for the shorter geometries (figures 5a/b) the core becomes increasingly perturbed and non-axial.

In part, this behaviour can be linked to flow at the entry to the vortex finder where, for the shorter geometries, the vortex core is inclined to the exit plane, thereby promoting localised reverse axial flow. As the solution evolves in time these instabilities eventually wash away for the longer domains (figures 5c/d) but prevail in the shorter domains and prevent the flow from settling into a stable flow pattern. This state can be classified in terms of flow criticality as a high swirl-number case, as discussed in [10]. According to their findings, swirling flows can have either a low or a high swirl number called either supercritical or subcritical respectively. In *supercritical* flows no information from a downstream point can be transported upstream, whereas in *subcritical* flows a downstream disturbance can propagate upstream hence changing the flow patterns there.

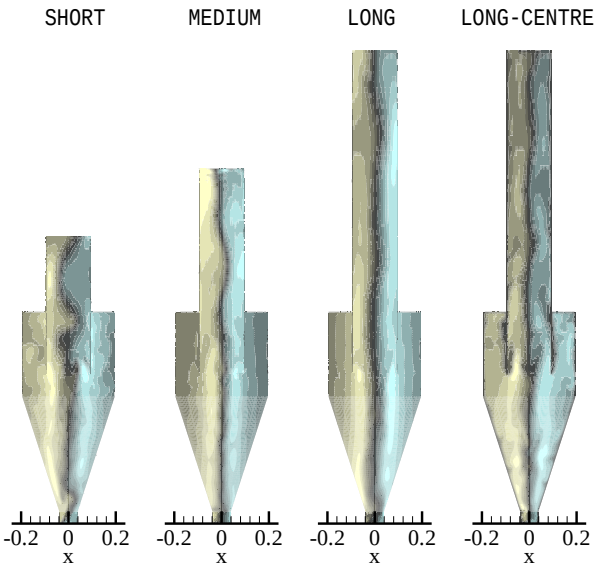

Figure 5: Location of the centre vortex for different exit tube geometries visualised by time-averaged swirl velocity: short (a), medium (b) and long (c) straight outlet; long with blocked centre part (d)

Figure 6 displays the axial velocity profiles in the vortex finder starting just downstream of the entry plane at $z^*/R \approx 0.5$. The velocity evens out the asymmetry linked to the swirl velocity and begins a recovery towards a rotating pipe flow. At the most downstream location (figure 6c) massive reverse flow occurs in the central part, resulting from by the strong vortex and the low pressure associated with it. As even the geometries with the longest exit tube have reverse flow at these locations, this reverse flow in itself cannot be the main reason for the lack of swirl observed in the short geometries. As only the blockage in the `LONG-CENTRE` geometry prevents this backflow, it seems to be entirely driven by low pressure in the vortex core.

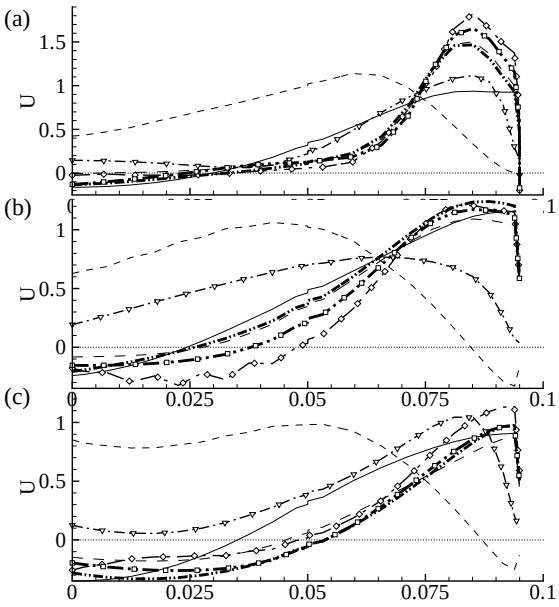

Figure 6: Time-averaged axial velocity profiles in the vortex finder at: (a) $z^*/R=1.0$, (b) $z^*/R=2.0$ and (c) $z^*/R=3.1$.

In figure 7 the swirl numbers $\langle S\rangle = (\int_0^R wur^2\,dr)/(R\int_0^R u^2\,r\,dr)$ in the vortex finder (averaged in the circumferential direction) are shown. While most solutions have rather high but almost constant swirl numbers just above $\langle$S$\rangle$=2, the low swirl of the SHORT domain can also be seen. The swirl number drops significantly in the short vortex finder (cf. figure 2a), indicating some kind of non-settled behaviour. The cases with longer exit tubes apparently have a more stable flow pattern owing to the distance of the exit from the cyclone itself, and hence disturbances originated in the outlet area do not tend to feed back into the main part of the cyclone chamber.

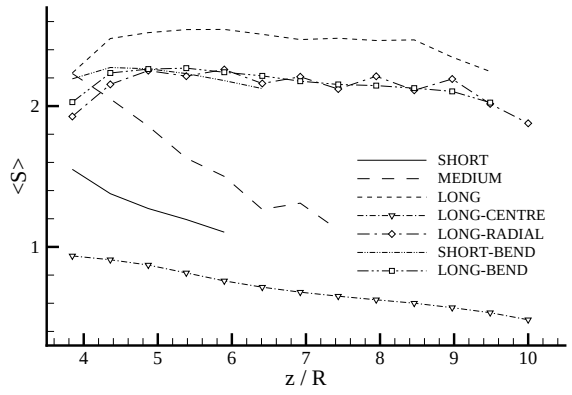

Figure 7: Swirl number $\langle$S$\rangle$ in the vortex finder averaged in the azimuthal direction at downstream locations; note that these values are only determined in the straight part of the exit tube.

Conclusions

Flow simulations of cyclones with different exit tube geometries have been carried out using detached eddy simulation. The DES method predicts the main flow properties quite accurately, however, depending on the length of the vortex finder two different flow pattern can be identified. In case of a short vortex finder, flow can enter the domain and alter the dynamics in the main cyclone chamber resulting in poor swirl velocities. In geometries with a longer vortex finder, these effects do not arise, although even for the geometries which include a bend, reverse flow can occur without any serious consequence on the overall results.

Acknowledgements

The support of the Australian Partnership for Advanced Computing (APAC) is gratefully acknowledged. Thanks are also due to R. Weber for his helpful suggestions.

References

[1] Boysan, F., Swithenbank, J. and Ayers, W. H., Mathematical modeling of gas-particle flows in cyclone separators, in *Encylopedia of Fluid Mechanics*, editor N. P. Cheremisinoff, Gulf, 1986, volume 4, 1307–1329.

[2] Griffiths, W. and Boysan, F., Computational fluid dynamics (CFD) and empirical modelling of the performance of a number of cyclone samplers, *J. Aero. Sci.*, **27**, 1996, 281–304.

[3] Schmidt, S., Blackburn, H., Rudman, M. and Sutalo, I., Simulation of Turbulent Flow in a Cyclonic Separator, in *3rd Int. Conf. CFD Minerals and Proc. Ind.*, editors P. Witt and M. Schwarz, CSIRO, Dec 10-12, Melbourne, Australia, 2003, 365–369, 365–369, ISBN 0 643 09037 1 (Printed Book).

[4] Schmidt, S. and Thiele, F., Comparison of numerical methods applied to the flow over wall-mounted cubes, *Intnl J. Heat Fluid Flow*, **23**, 2002, 330–339.

[5] Schmidt, S. and Thiele, F., Detached Eddy Simulation of Flow around A-Airfoil, *J. Flow Turbulence & Combustion*, **71**, 2003, 261–278.

[6] Spalart, P. and Allmaras, S., A one-equation turbulence model for aerodynamic flows, *La Rech. Aérospatiale*, **1**, 1994, 5–21.

[7] Spalart, P., Jou, W.-H., Strelets, M. and Allmaras, S., Comments on the feasibility of les for wings, and on a hybrid rans/les approach, in *Advances in DNS/LES*, editors C. Liu and Z. Liu, Greyden Press, Columbus, OH, USA, 1997.

[8] Strelets, M., Detached Eddy Simulation of Massively Separated Flows, in *39th AIAA Aerospace Sciences Meeting and Exhibit*, AIAA, Reno, Nevada, 2001, number 2001-0879 in 2001-0879, #2001-0879.

[9] Sutalo, I. and Merrell, J., Pressure loss measurements on physical models of cyclones, Report 99/095, CSIRO BCE, 1999.

[10] Weber, R., Visser, B. and Boysan, F., Assessment of turbulence modeling for engineering prediction of swirling vortices in the near burner zone, *Intnl J. Heat Fluid Flow*, **11**, 1990, 225–235.

[11] Xue, L., *Entwicklung eines effizienten parallelen Lösungsalgorithmus zur dreidimensionalen Simulation komplexer turbulenter Strömungen*, Dissertation, Technische Universität Berlin, 1998.